Making Use of Process Tomography Data for Multivariate Statistical Process Control

Bundit Boonkhao, Rui F. Li, and Xue Z. Wang
Institute of Particle Science and Engineering, School of Process, Environmental and Material Engineering, University of Leeds, Leeds LS2 9JT, U.K.

Richard J. Tweedie, and Ken Primrose
Industrial Tomography Systems Limited, Speakers House, 39 Deansgate, Manchester M3 2BA, U.K.

DOI 10.1002/aic.12443
Published online November 9, 2010 in Wiley Online Library (wileyonlinelibrary.com).

A novel strategy for making effective use of on-line process tomography measurements for process monitoring is described. The electrical resistance tomography (ERT) sensing system equipped with sixteen electrodes provides 104 conductivity measurements every 25 ms. The data has traditionally been used for construction of images for display purpose. In this study, ERT data was used for multivariate statistical process control. Data at predefined normal operational conditions was processed using principal component analysis. The compressed data was used to derive two statistics, T^2 and squared prediction error (SPE). T^2 and SPE charts predict the probability that the process being monitored has undergone statistically significant changes from previous state or the so-called normal operational state, in terms of mixing quality. The methodology is illustrated by reference to a case study of a sunflower oil/water emulsion process. © 2010 American Institute of Chemical Engineers *AIChE J,* 57: 2360–2368, 2011
Keywords: electrical resistance tomography, multivariate statistical process control, principal component analysis, emulsion

Introduction

Process tomography is now an established imaging technique for studying the mixing behavior of multiple phase fluid systems in vessels and pipelines.[1–4] It samples a substantial proportion of the process volume rather than at a single point; therefore, it is particularly useful for investigating the dynamic performance of a manufacturing process. Among various process tomography techniques, electrical resistance tomography (ERT) is one of the most established and widely used. It comprises a sensor array, a data acquisition system, and a personal computer with control and data processing software.[4] The sensor array consists of multiple electrodes arranged around or within the region of interest at fixed locations in such a way that they make electrical contact with the fluid inside the vessel without interfering the flow or movement of materials. The most common configuration is a circular pipe or vessel with 16 electrodes as shown in Figure 1. The data acquisition system injects current between electrode pairs and measures the resulting voltages on electrode pairs according to a predefined measurement strategy. Common strategies include the adjacent and opposite. Figure 1 represents the adjacent strategy, according to which current is injected between an adjacent pair of electrodes and voltage is measured at remaining adjacent pairs of electrodes (excluding the injection pair). The injection pair is switched until all independent combinations have been completed. A 16-electrode sensor array provides 104 independent measurements for this protocol. Then the electrical conductivity tomography (or distribution) within the sensing zone can be displayed by applying an image reconstruction algorithm to the measured voltages.

Correspondence concerning this article should be addressed to X. Z. Wang at x.z.wang@leeds.ac.uk.

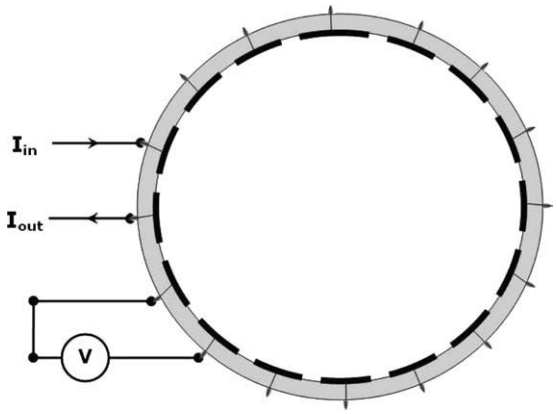

Figure 1. The electrical resistance tomography.

ERT has become an acceptable technique for investigating, monitoring, and controlling industrial processes. There has been a wealth of literature reporting successful use of ERT in industrial applications. Lucas et al.[5] reported the use of a dual-plane ERT system for measuring the local solid-volume fraction distribution and the local solid-axial velocity distribution in solid–liquid flows. Wang et al.[6] applied ERT to measure the formation and characteristics of asymmetric solids distributions and particle trajectories in a horizontal pipe subjected to swirling flows. Mann et al.[7] applied ERT to the investigation of the mixing behavior of a plant scale stirred tank for detection of the air-core vortex and dynamic behavior of miscible fluid mixing and gas–liquid mixing. Sun et al.[8] applied ERT to concentration measurement in a cyclone dipleg. Holden et al.[9] also used the ERT to observe several pathological mixing behavior caused by equipment malfunction inside a plant scale stirred vessel, such as settling at the vessel base, accumulation behind baffles, and settling on the impeller. Authors are referred to a recent review for more information about ERT application for wet particulate processing.[4]

Through visual inspection on the reconstructed conductivity tomography images, process operating condition is monitored. Abnormalities in the vessels or pipelines, such as settlement of particles in some zones, can be detected. The detection accuracy clearly relies on the quality of the reconstructed images, which is dependent on the algorithm and conductivities of two phases of the fluid used in the image reconstruction process. In addition, it might not be always straightforward for a user (e.g., a process engineer) to make judgment on the process status by visually inspecting the images which update continuously in real-time. When there is a perceived change in process condition, it can be challenging to assess the significance of the change, e.g., on the judgment if this means moving into an abnormal operational state.

This article presents a methodology for making novel use of ERT measurements for multivariate statistical process control (MSPC). It uses the raw measurements of the 104 voltages, to derive two statics T^2 and squared prediction error (SPE). T^2 and SPE charts predict the probability of the monitored process being at normal or abnormal operational state and can be used for 6σ process control.

The rest of the article is organized as follows. The materials and instrument used and experiments conducted are described in the next section. The MSPC model based on ERT measurements is introduced in Results and Discussions section. Results of applying the MSPC model to a case study process in our Particle Manufacturing Laboratory, a sunflower oil–water emulsion manufacturing rig, are presented in Final Remark section, which is followed by conclusions in the final section.

Experiments

Schematic of the experimental system

The experimental system is shown in Figure 2. The system combines an ultrasound sensor and an ERT sensor to realize the simultaneous measurements of particle size, concentration, and the visualization of flow pattern of the emulsion, whereas the process of emulsification continues. It mainly contains three parts: a cross flow membrane emulsification rig (Figure 3) that generates emulsions, an emulsion tank for storage of emulsions made, and a circulation loop through which the emulsions were pumped out of the emulsion tank and returned to the tank. On the circulation loop, an ERT sensing system and an ultrasound spectrometer (USS) were installed. USS was used for measuring droplet-size distribution of the dispersed phase. In addition to ERT and USS, there are other sensors for measurements of pH, conductivity, temperature, and flow rate in the circulation loop. The ERT sensor not only is used for charactering mixing behavior but also provides concentration information as a critical parameter for the particle-size distribution analysis with the USS spectrometer. The flow rate of the emulsion in the circulation loop where ERT and USS are mounted is set to be 0.25 m/s.

Crossflow membrane emulsification

Membrane emulsification is a technique for size-controlled production of particulates thus became a very important process for food, chemical, cosmetics, and pharmaceutical industries. The development of this technique can be traced back to late 1980s, its recent progress can be found in a review by Vladisavljevic and Williams.[10] Crossflow membrane emulsification is a method by which the dispersed phase flows through the porous membrane from one side of its surface to the other to form droplets and these droplets are

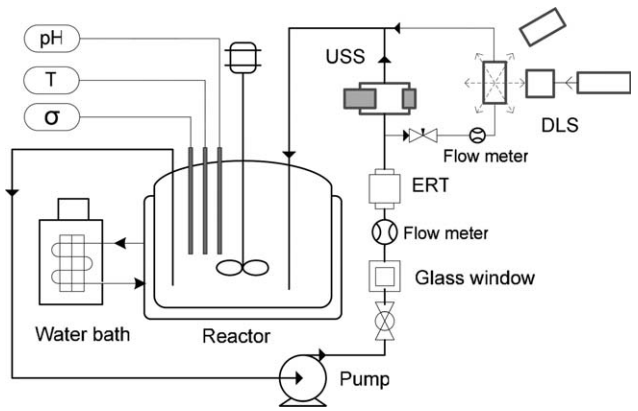

Figure 2. The flow diagram of the experimental rig used in this study.

ERT, electrical resistance tomography; DLS, dynamic light scattering; USS, ultrasound spectroscopy.

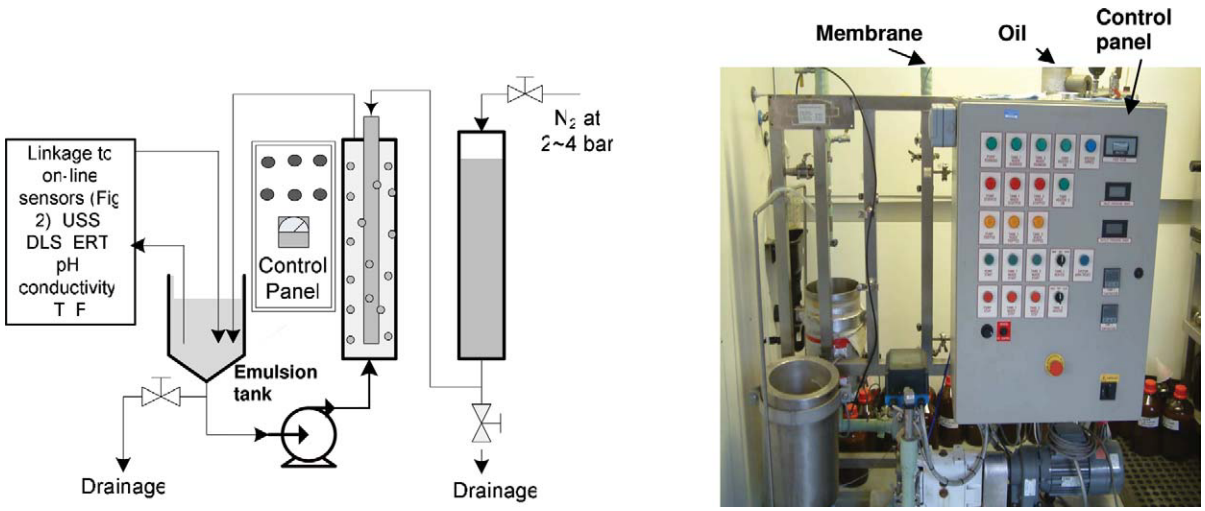

Figure 3. The emulsion rig used in this study.

[Color figure can be viewed in the online issue, which is available at wileyonlinelibrary.com.]

then scoured away by the cross flow of the continuous phase. In this way, the emulsion can be manufactured under lower shear conditions than with conventional emulsification techniques and the droplet-size distribution can be largely controlled through the choice of the pore size and size distribution of the membrane and the flow conditions of the continuous phase.

The main components, as shown in Figure 3, of a typical crossflow membrane emulsification apparatus normally include a continuous-phase circulation loop, a membrane module, a dispersed-phase tank, a pressurizing source, and a control panel. The circulation loop mainly contains a tank to store the continuous phase and the emulsion product and a pump to provide the driving force for circulation to scour away droplets formed on the surface of the membrane to form emulsion. The membrane module contains a membrane and a container to hold the membrane under high pressure. The dispersed-phase tank is used to store the dispersed phase and able to hold high pressure. The membrane module is connected to both dispersed-phase tank and the circulation loop. The pressurizing source provides high-pressure air to push the dispersed phase from its storage tank through the membrane into the circulation loop. Finally, the control panel provides the control for power connection and the flow of the continuous phase.

The size and size distribution of the emulsion droplets largely depend on the pore size and pore-size distribution of the membrane. There is no rigorous quantitative relationship between them. However, in general, the final mean droplet size would be expected to be 2–8 times of the average pore size of the membrane depending on the type of the membrane (materials and wettability to the dispersed and continuous phases), pressure applied, surfactant used, and process conditions such as flow rate of the continuous phase and temperature.

Electrical resistance tomography

For details for the mechanisms of operation of the USS, readers are referred to a recent publication.[11] Although ERT was also introduced in the reference, for better readability of this article, here we still briefly describe the ERT system used. The ERT system used was a standard circular sensor with 16-electrods developed by Industrial Tomography Systems,[12] as shown in Figure 1. The diameter of the ERT vessel is 4.5 cm. In total, 16 electrodes are arranged at equal intervals in the same plane around the periphery of the circular vessel. Current is applied through two neighboring electrodes, and the voltages are measured from the remaining pairs of neighboring electrodes. The procedure is repeated until all the independent measurements have been made. The adjacent measurement strategy yields N^2 measurements, where N is the number of electrodes. However, of these only $N(N-1)/2$ are independent. To avoid electrode contact impedance problems, the voltage is not measured at a current-injecting electrode, and therefore, the total number of independent measurements is reduced to $N(N-3)/2$. Therefore, a 16-electrode sensor gives 104 independent measurements. These voltages are then converted into conductivities to construct an image showing conductive and nonconductive regions.

Materials and experimental conditions

Sunflower oil was used as the dispersed phase, whereas 2 wt % sodium dodecyl sulfate surfactant aqueous solution is the continuous phase with a conductivity 2.59 mS/cm and pH 6.5 at temperature 25°C. For the sunflower oil, the density is 0.93 g/cm^3 and viscosity is 6.43×10^{-2} Pa/s^{-1}. Other physical properties required by USS for particle-size distribution are: ultrasound speed 1.77×10^3 m/s, thermal dilation 6.67×10^{-4} m^3/K, thermal conductivity 0.17 W/m/K, specific heat 1.98 J/kg/K, and attenuation coefficient $42.52f^{1.69}$ dB/m, where f refers to frequency. The emulsification was carried out continuously at room temperature around 25°C. The flow rate of the continuous phase, i.e., the flow rate between the emulsion tank and the membrane, was kept constant at 539 l/min. The membrane tube used has an average pore size of 0.2 μm. The pressure pushing the oil through the membrane into the continuous phase varied from 3.0 to 5.5 bar along with the continuous experiment. The continuous phase (SDS solution) was filled in the emulsion tank as labeled in Figure 3, then it is pumped around to fill

in all the process lines. Although the continuous phase is thus circulated in the process lines, N_2 is switched on to compress the oil membrane holes into the continuous phase. When the concentration of the emulsion reaches the target value, N_2 is switched off to stop pushing oil into the emulsion. The emulsion concentration in circulation will, therefore, be kept constant. It is from this point that the tomography measurements are used for the study in this work. At this constant concentration, clearly circulation flow rate can still be adjusted. To produce emulsions of different concentrations, the same procedure is followed. During the experiments, solution concentrations and flow rates were changed. The flow rate change covers 0.190, 0.166, 0.133, 0.108, 0.083, 0.055, and 0.041 l/s. The volume concentration change covers 33%, 30%, 25%, 20%, 15%, 10%, 5%, 3%, 2%, and 1% volume concentration.

MSPC models using ERT data

Process conditions need to be monitored so that major disturbances can be detected and diagnosed as early as possible before appropriate actions can be taken. MSPC based on Hotelling's T^2 and SPE charts are key techniques for this purpose.

A significant development in MSPC has been the introduction of principal component analysis (PCA) for compression of data before deriving.[13,14] PCA uses a projection technique that transforms the original data to some latent variables, principal components (PCs). The number of PCs depends on how much the PCs retain the variance of the original data. The transformation can be described using the following equation:

$$\mathbf{X} = \mathbf{T}\mathbf{P}^{\mathbf{T}} + \mathbf{E} \tag{1}$$

where $\mathbf{X}[m \times n]$ is the normal operational data matrix which composes of m observations about n process variables, $\mathbf{T}[m \times k]$ is the score matrix, $\mathbf{P}[n \times k]$ is the loading matrix, and $\mathbf{E}[m \times n]$ is the error matrix. For MSPC, the first few PCs, k PCs, are used rather than the original variables. This means that k dimensions are used instead of n dimensions in loading matrix, $\widehat{\mathbf{P}}[k \times n]$. When the new observation obtains, $\mathbf{x}[1 \times n]$, the new score vector, $\mathbf{t}[1 \times k]$, can be calculated by

$$\mathbf{t} = \mathbf{x}\widehat{\mathbf{P}}^{\mathrm{T}} \tag{2}$$

Then, the first statistic monitoring, Hotelling's T^2, can be calculated by

$$T^2 = \sum_{i=1}^{k} \frac{t_i^2}{S_{t_i}^2} \tag{3}$$

where t_i is the score of ith process variable, $S_{t_i}^2$ is the estimated variance of t_i and k the number of retained PCs.

The second statistic monitoring aims to monitor the absence of the information by SPE:

$$\mathrm{SPE} = \sum_{i=1}^{k} (y_{\mathrm{new},i} - \widehat{y}_{\mathrm{new},i})^2 \tag{4}$$

where $\widehat{y}_{\mathrm{new},i}$ and $y_{\mathrm{new},i}$ are the reconstructed value of the ith process variable from the reference PCA model and the measured value of this variable, respectively. SPE is also referred as Q-statistic or distance to the model.

The meaning of the Hotelling's T^2 and SPE can be described by the distance definition approach. The Hotelling's T^2 is defined as the distance from the measured data to the mean which is called Mahalanobis distance. In other words, the Hotelling's T^2 monitors the dispersion of data around the mean. For SPE, it is defined as the distance difference between data predicted from model and data from measurement. It can be said that SPE is the error between the original measured data and predicted data from MSPC.

Control limits for both statistical monitoring charts can be set as 95%, 97%, or 99%. Care has to be taken for setting the control limit for SPE chart, because as Louwerse and Smilde[15] discovered in a study for fault detection of batch processes, unlike T^2 charts, the SPE control limit is very difficult to set as either 99% or 99.9%. In the case studies to be presented in the next section, the control limits for T^2 and SPE charts are set as 99%.

There are various variations of MSPC models depending on the PCA method being linear or nonlinear,[16,17] the way of scaling the data, whether it is used together other techniques such as wavelets[18] and inductive data mining,[19,20] using PCA or independent component analysis for dimension reduction[21–26] as well as the process being continuous or batch.[27] Comprehensive review of research in this area has been made by a number of researchers.[20,28–30] Readers are referred to these review papers and books for further details of the methods. The procedure of developing MSPC models for monitoring mixing conditions using ERT tomography data are described below.

First, historical ERT data at predefined normal operational conditions in terms of mixing is collected. Because MSPC was aimed at detecting abnormal events, it requires a normal operational state to be defined and data collected to build the MSPC models. As a matter of fact, MSPC models can be built using data representing any specific operational state, not necessarily real normal operation state. It can then be used to detect the probability of an event that is abnormal in comparison with the data used in MSPC model construction.

The collected historical data has to be preprocessed before further analysis. In here, the word "frame" is first introduced. These 104-voltage measurements (indication of 104 conductivities) are analogues to the traditional sensor measurements of temperature, pressure, and flow rate used in traditional MSPC models. For every frame, the 104 measurements were scaled using the following equation:

$$V_{\mathrm{new}}(p,q) = \frac{V_{\mathrm{raw}}(p,q) - V_{\min}(p)}{V_{\max}(p) - V_{\min}(p)} \qquad (q = 1, 2, 3, \ldots, 104) \tag{5}$$

where $V_{\mathrm{new}}(p,q)$ and $V_{\mathrm{raw}}(p,q)$ are the qth preprocessed and raw voltage measurements, respectively, on the pth frame, $V_{\min}(p)$ and $V_{\max}(p)$ are the minimum and maximum raw values on the pth frame, respectively. For each frame, the 104 voltage measurements give information about the distribution of conductivity values across the cross-sectional area of the pipe. The scaling using Eq. 5 for each frame makes such information for all frames comparable. After scaling voltage for every frame, auto-scaling is applied for normalization of the data for all frames, to make each measurement has the same variance. Auto-scaling is a standard step in normal-

ization of data that makes the standard deviation to unit by scaling (dividing) all the values by the standard deviation of the original data, more detail can be found in Wold et al.[31]

PCA is subsequently applied to the preprocessed data. The data was decomposed into linear combination form, Eq. 1. There are various techniques and software systems for analyzing PCA, e.g., MATLAB, SIMCA-P, and WEKA. Then, the MSPC models for Hotelling's T^2 and SPE are developed by using the selected PCs, instead of the original 104 measurements, as described by Eqs. 3 and 4.

When new measurement frames are obtained, the MSPC model is applied for monitoring mixing condition. The new frames need to be preprocessed by scaling over each frame using Eq. 5, and normalizing for all frames via auto-scaling as described above. The scores of new frames were calculated using Eq. 2 with the appropriated number of k. Consequently, the new scores were used for predicting their Hotelling's T^2 and SPE. Plotting of Hotelling's T^2 and SPE on a chart in association with control limits represents the MSPC chart, which can be used as monitor for tracking the mixing condition. If both statistical indices are bounded under control limit, it means that the system is statistically in control. Otherwise, if either index is over bounded their control limit, the system is undergone in a way of out-of-control or an abnormal event occurring. Fault diagnosis and identification should then be applied. The next section will present monitoring charts for ERT data of sunflower oil/water emulsion.

Results and Discussions

The tomography voltage measurements at flow rates 0.166, 0.133, and 0.108 l/s of concentrations from 33% to 5% were used as normal operational data to develop the PCA-based MSPC models. Remember that the MSPC models were developed for monitoring mixing behavior only. Here, the mixing behavior is characterized by the distribution of conductivity over the cross-sectional area of the pipe where electrodes were mounted. If the conductivity is uniformly distributed, it is regarded as good mixing; if the conductivity in part of the cross-sectional area of the pipe is significantly lower or higher than in other parts of the cross-sectional area, the mixing is considered as poor. The total data of 23,768 frames (each with 104 voltage measurements) was collected for MSPC model development. The data was preprocessed first for each frame using Eq. 5 and then for all frames via auto-scaling, as described in the previous section. PCA was applied to the preprocessed data to develop the MSPC models. The result showed 20 PCs were needed, which explained about 73% variance of the data. Finally, the 20 PCs are used to construct MSPC monitoring charts.

The MSPC models obtained was applied for monitoring new operations. Figure 4 shows an example for the emulsion at 20% of concentration and various flow rates. It can be seen that significant increases of both SPE and Hotelling's T^2 occurred after the flow rate was reduced to below 0.055 l/s, and both values have exceeded the 99% control limits. This indicates that there is 99% probability that the mixing behavior became poor below this flow rate. This detected event of moving away from the predefined normal mixing condition can also be clearly seen in the PC1 $\sim$ PC2 scatter plot, as shown in Figure 5, where the PC1 $\sim$ PC2 projections of the

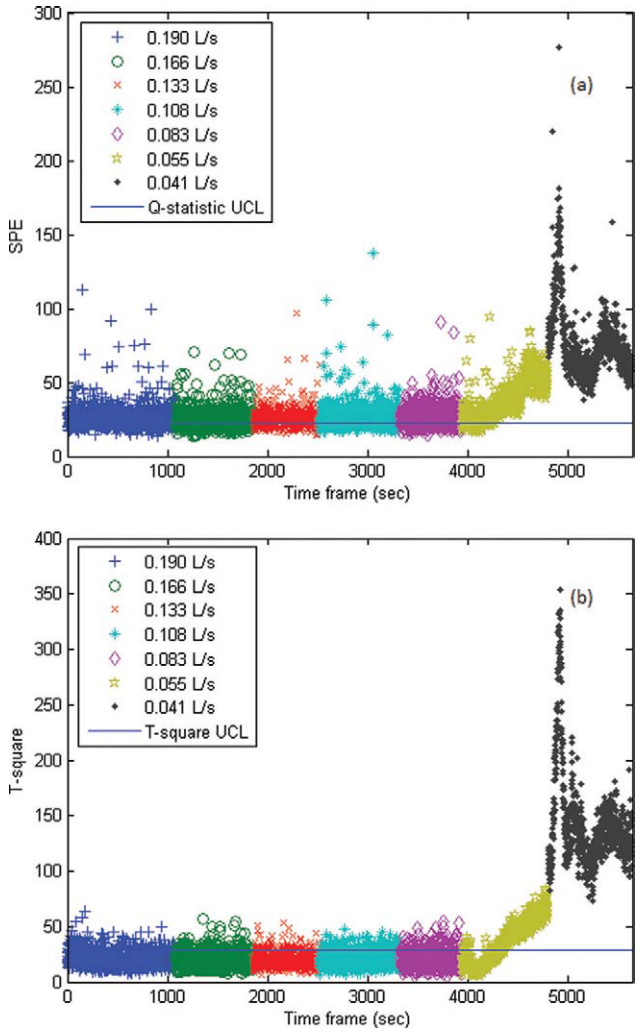

Figure 4. Monitoring charts for the sunflower oil–water emulsion at concentration 20% and different flow rates, (a) SPE and (b) T^2.

[Color figure can be viewed in the online issue, which is available at wileyonlinelibrary.com.]

tomography measurements at high-flow rates on the PC1 $\sim$ PC2 plane are grouped into one cluster, whereas the points at lower flow rates are out of this cluster (points representing flow rates of 0.055 l/s and 0.041 l/s). Figure 6 shows the reconstructed conductivity tomography during the period of flow rate reduction (from 0.055 l/s to 0.041 l/s), from which the poor mixing can be clearly observed when flow rate is reduced. It is worth noting that the images in this figure were reconstructed using a fixed color-scaling template rather than the color template originally used by the on-line tomography instrument. The on-line instrument uses a changeable color scale for maximally visualizing the difference within a single image. Here probably, it is not appropriate to call the deviation of 0.055 l/s as a fault. It is just that at this low-flow rate, the conductivity across the cross-sectional area of the pipe becomes no longer uniform, indicating poor mixing. This could in future help flow pattern analysis, e.g., different flow regimes, bubble, slug, multiple bubble and annular flow regimes.

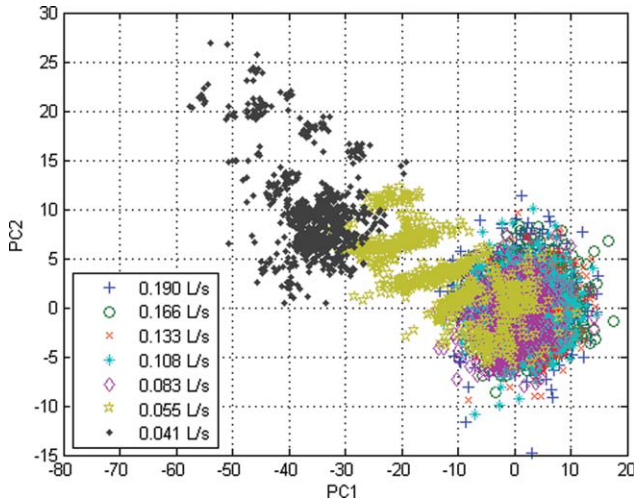

Figure 5. The projection of tomography measurements on the PC1 ~ PC2 plane for sunflower oil–water emulsion at concentration 20% and different flow rates.

[Color figure can be viewed in the online issue, which is available at wileyonlinelibrary.com.]

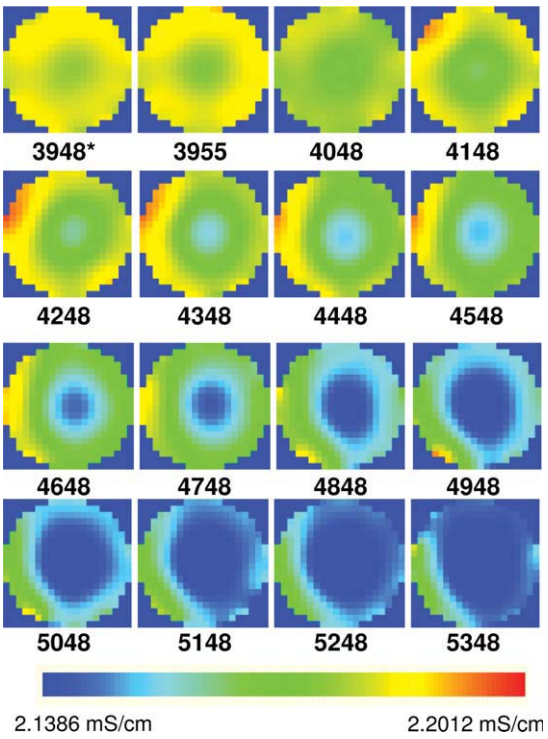

Figure 6. The change of the reconstructed conductivity tomography at fixed color scale for some frames of the sunflower oil–water emulsion at concentration 20% due to the change of flow rate ("*" the number at bottom of each image is the time stamp for the image).

[Color figure can be viewed in the online issue, which is available at wileyonlinelibrary.com.]

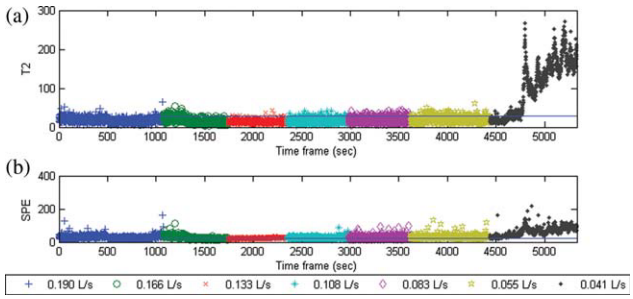

Figure 7. The monitoring charts for the sunflower oil/water emulsion at 15% of concentration and different flow rates, dash line is 99% upper control limit of individual control chart.

(a) Hotelling's T^2 and (b) square prediction error charts. [Color figure can be viewed in the online issue, which is available at wileyonlinelibrary.com.]

As well as for the emulsion at concentration 15%, the Hotelling's T^2 and SPE monitoring charts at different flow rates are shown in Figure 7. It was shown that there are two time periods where the SPE exceeded its control limit, in one of which, both SPE and T^2 exceeded their control limits. The first increase in SPE occurred at the beginning of experiment and at 0.190 l/s of flow rate. During this time, a certain amount of sodium dodecyl sulfate solution was added into the reactor to produce the emulsion with a lower concentration. This dilution process might have caused the mixing state of the emulsion to become different. The second period with a significant increase in SPE is located at the time when the flow rate was changed from 0.190 l/s to 0.166 l/s. This sudden change at flow rate could have been the course led to the change of mixing behavior.

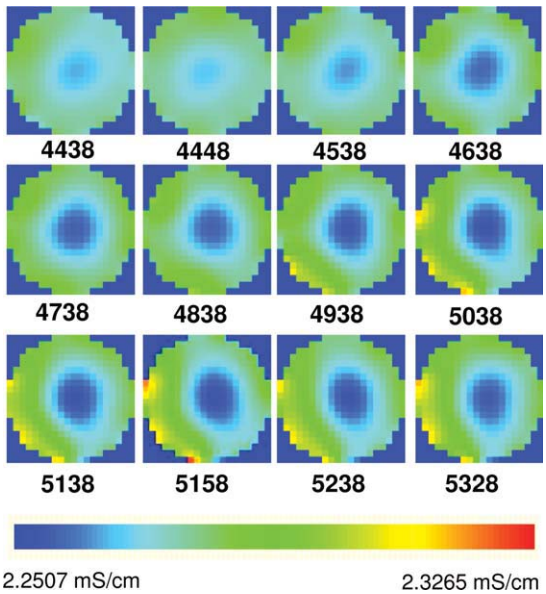

Figure 8. The change of the reconstructed conductivity tomography of the sunflower oil/water emulsion flow using fixed color scale at concentration 15% and at the different flow rates.

[Color figure can be viewed in the online issue, which is available at wileyonlinelibrary.com.]

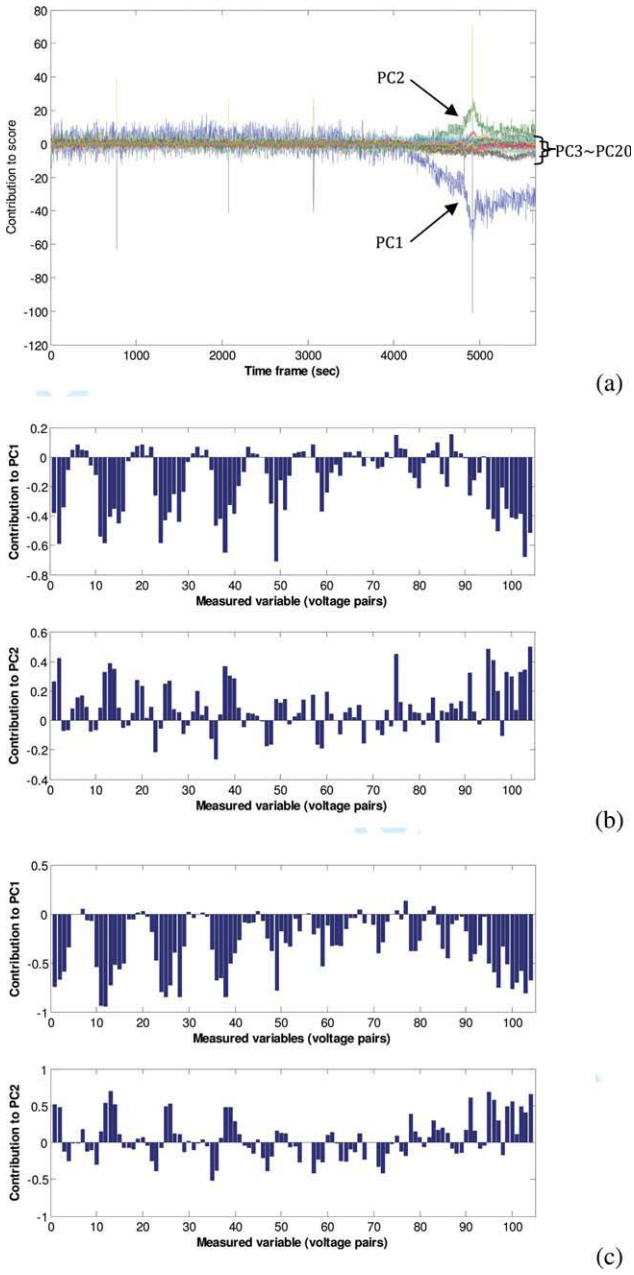

Figure 9. The contribution plots of scores at concentration 20%.

(a) Score plot of 20 selected PCs at various flow rates, (b) contribution plots to PC1 and PC2 by 104 voltage measurements at frame 4748 (flow rate 0.055 l/s), and (c) contribution plots to PC1 and PC2 of 104 voltage measurements at frame 5248 (flow rate 0.041 l/s). [Color figure can be viewed in the online issue, which is available at wileyonlinelibrary.com.]

The period with an increase in both SPE and T^2 occurred at the flow rate 0.041 l/s. This low-flow rate might have caused the oil particles to be separated into an area, as demonstrated from the reconstructed conductivity tomography images, Figure 8, where more oil particles are gathered in the central area.

Because Hotelling's T^2 is calculated by the summation of squared scores (Eq. 3), the cause of out-of-control can be diagnosed using score contribution analysis. The methodology of performing score contribution is discussed in detail in literature.[32] In the first step, score plots are used to identify the latent variables, i.e., PCs that contributed most to out-of-control of T^2 statistic. Figure 9a shows the score plots for the 20 PCs to T^2 at different time frames for the emulsion concentration of 20%. It can be seen that at around time frame of 4748, where T^2 is out of control as shown in Figure 7a, PC1 and PC2 have shown to give higher contribution than PC3 $\sim$ PC20. This is indication that the cause of out-of-control in T^2 at time frame 4748 was most likely due to PC1 and PC2. Once the PCs are identified, the next step is to find the original process variables. This can be achieved by plotting the contribution plots of scores of original process variables to PCs1 and PC2. Figures 9b, c show the plots of scores of each process variable (i.e., the voltage pair) on PC1 and PC2 at time frame 4748 (flow rate 0.055 l/s) and 5248 (flow rate 0.041 l/s), respectively. A cluster of measured voltage pairs are found to be responsible. For contribution to PC1 by original variables, Figures 9b, c, there are six sets of the voltage pairs that give high contributions to PC1.

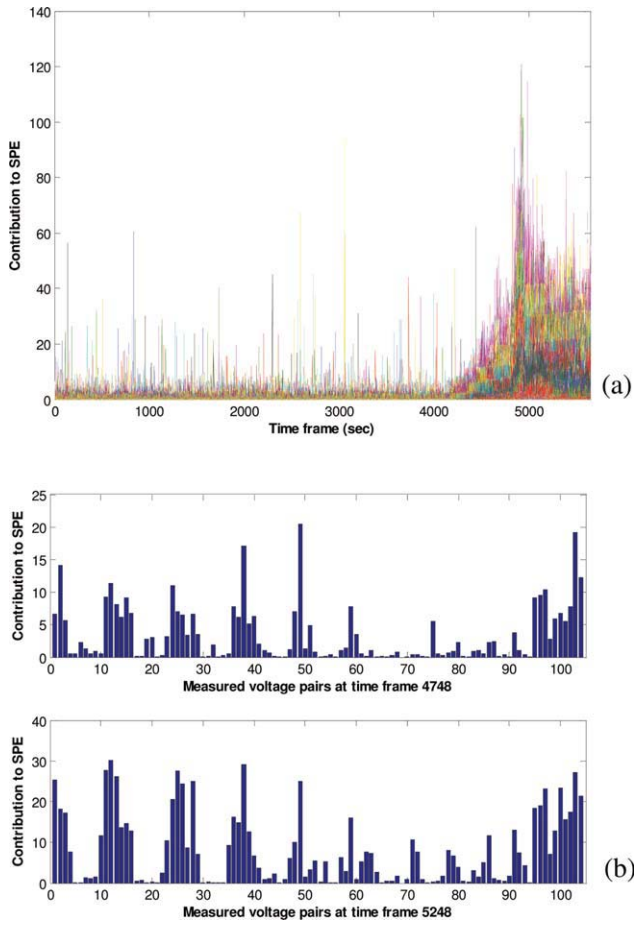

Figure 10. Contribution plots of squared prediction error at concentration 20%.

(a) Contribution to SPE for all PCs over time frames. (b) Top: contributions to SPE at time frame 4748 (flow rate 0.055 l/s); bottom: contributions at time frame 5248 (flow rate 0.041 l/s). [Color figure can be viewed in the online issue, which is available at wileyonlinelibrary.com.]

They are set A[1–4], B[11–16], C[23–29], D[36–40], E[48–51], and F[95–104] noting that the numbers in square bracket refer to measured voltage pairs. In the case of contribution analysis to PC2, Figures 9b, c, even if they are not clearly identified the sets of variables, they can also be grouped as cluster-like PC1 because the variables in the same sets of PC1 also have high contributions. Therefore, it can be concluded that the sets A–F of measured voltage pairs are identified as the causes.

To find out the root cause of abnormal event detected by SPE, e.g., Figure 7b at time frame around 4748, score contribution plots similar to T^2 can be performed.[32,33] The first step is to identify the contributing PCs. Figure 10a shows the score contribution plots of PCs to SPE over a set of time series for the emulsion concentration of 20%. Figure 10a shows that at around time frame 4748 it was found difficult to identify which PCs are dominant. As a result, contribution plots to SPE by original measured variables are analyzed. The plots of Figure 10b are contributions of original variables at time frame 4748 (flow rate 0.055 l/s) and 5248 (flow rate 0.041 l/s), respectively. It can be seen that measured voltages which highly contribute to SPE are grouped and identified as the sets of voltages A–F. This result is consistent to the contribution analysis for T^2.

The contribution plots presented above have only related poor mixing to the voltage pairs of the electrodes. It would be more meaningful if it is able to relate to such kind of process variables as flow rate and pressures, though it is not clear how this can be done for the case studies presented in here. Nevertheless, the methodology of performing contribution analysis can be useful for some other purposes. For example, it is possible to make use of process tomography based MSPC monitoring and contribution plots presented above to correlate mixing behavior with flow regimes such as bubble, slug, multiple bubble, and annular flow regimes. Dong et al.[34] had presented interesting attempts to correlate the measurements of voltage pairs with flow regimes. The work MSPC and contribution plots approach presented in this work have potential advantages because it is an unsupervised method, therefore does not need training.

Final Remarks

Multiple sensors of electrical resistance process tomography (ERT) provide real-time information about process conditions, e.g., mixing behavior. In this study, the ERT system has 16 electrodes that give measurements of 104 voltages every 25 ms. Traditionally, the measurements have been used to reconstruct color images to be visually displayed to users. In this study, it was proposed to make use of the tomography data for MSPC. MSPC gives the probability, i.e., a statistical confidence level, of e.g., 99% depending on how the control limit is set, of a predicted or perceived event being abnormal. This is clearly advantageous than purely relying on observation by human operators of the reconstructed images for monitoring purpose, not only because continuous observation by human operators of the ever updating images is challenging as MSPC-based monitoring is tireless but also because sometimes, it is difficult for an human expert to make conclusions, in a quantitative way, if a perceived event is abnormal. The study has demonstrated the methodology by developing MSPC charts for monitoring mixing behavior for processing oil/water emulsions. The results have been shown that at the low-flow rates the mixing condition was poor as detected by the MSPC chart. The diagnosis of variables that caused the system out-of-control can be represented as a set of measured voltages pairs of ERT system.

Acknowledgments

The authors thank the financial support from the Technology Strategy Board (TP/SC/6/I/10097) and UK Engineering and Physical Sciences Research Council (Grant numbers: EP/E040624/1 and EP/H008853/1).

Literature Cited

1. Wang M. Seeing a new dimension—the past decade's developments on electrical impedance tomography. *Prog Nat Sci*. 2005;15:1–13.
2. Williams RA, Beck MS. *Process Tomography: Principles, Techniques, and Applications*. Butterworth-Heinemann: Oxford, 1995.
3. Williams RA, Jia X. Tomographic imaging of particulate systems. *Adv Powder Technol*. 2003;14:1–16.
4. Stanley SJ, Bolton GT. Review of recent electrical resistance tomography (ERT) applications for wet particulate processing. *Part Part Syst Char*. 2008;25:207–215.
5. Lucas GP, Cory J, Waterfall RC, Loh WW, Dickin FJ. Measurement of the solids volume fraction and velocity distributions in solids-liquid flows using dualplane electrical resistance tomography. *Flow Meas Instrum*. 1999;10:249–258.
6. Wang M, Jones TF, Williams RA. Visualisation of asymmetric solids distribution in horizontal swirling flows using electrical resistance tomography. *Chem Eng Res Des*. 2003;81:854–861.
7. Mann R, Dickin FJ, Wang M, Dyakowski T, Williams RA, Edwards RB, Forrest AE, Holden PJ. Application of electrical resistance tomography to interrogate mixing processes at plant scale. *Chem Eng Sci*. 1997;52:2087–2097.
8. Sun M, Liu S, Li ZH, Lei J. Application of electrical capacitance tomography to the concentration measurement in a cyclone dipleg. *Chin J Chem Eng*. 2008;16:635–639.
9. Holden PJ, Wang M, Mann R, Dickin FJ, Edwards RB. On detecting mixing pathologies inside a stirred vessel using electrical resistance tomography. *Chem Eng Res Des*. 1999;77:709–712.
10. Vladisavljevic GT, Williams RA. Recent developments in manufacturing emulsions and particulate products using membranes. *Adv Colloid Interface Sci*. 2005;113:1–20.
11. Wang XZ, Liu LD, Li RF, Tweedie RJ, Primrose K, Corbett J, McNeil-Watson FK. Online characterisation of nanoparticle suspensions using dynamic light scattering, ultrasound spectroscopy and process tomography. *Chem Eng Res Des*. 2009;87:874–884.
12. ITS. Industrial Tomography Systems. 2008. Available at: www.itoms.com. Accessed September 10, 2009.
13. MacGregor JF, Kourti T. Statistical process control of multivariate processes. *Control Eng Pract*. 1995;3:403–414.
14. Albazzaz H, Wang XZ. Statistical process control charts for batch operations based on independent component analysis. *Ind Eng Chem Res*. 2004;43:6731–6741.
15. Louwerse DJ, Smilde AK. Multivariate statistical process control of batch processes based on three-way models. *Chem Eng Sci*. 2000;55:1225–1235.
16. Dong D, McAvoy TJ. Nonlinear principal component analysis—based on principal curves and neural networks. *Comput Chem Eng*. 1996;20:65–78.
17. Kramer MA. Nonlinear principal component analysis using autoassociative neural networks. *AIChE J*. 1991;37:233–243.
18. Bakshi BR. Multiscale PCA with application to multivariate statistical process monitoring. *AIChE J*. 1998;44:1596–1610.
19. Yuan B, Wang XZ. Multilevel PCA and inductive learning for knowledge extraction from operational data of batch processes. *Chem Eng Commun*. 2001;185:201–221.
20. Wang XZ. *Data Mining and Knowledge Discovery for Process Monitoring and Control*. London: Springer, 1999.
21. Albazzaz H, Wang XZ. Historical data analysis based on plots of independent and parallel coordinates and statistical control limits. *J Process Control*. 2006;16:103–114.

22. Lee JM, Qin SJ, Lee IB. Fault detection and diagnosis based on modified independent component analysis. *AIChE J*. 2006;52:3501–3514.
23. Albazzaz H, Wang XZ. Statistical process control charts for batch operations based on independent component analysis. *Ind Eng Chem Res*. 2004;43:6731–6741.
24. Lee JM, Yoo C, Lee IB. Statistical monitoring of dynamic processes based on dynamic independent component analysis. *Chem Eng Sci*. 2004;59:2995–3006.
25. Kano M, Tanaka S, Hasebe S, Hashimoto I, Ohno H. Monitoring independent components for fault detection. *AIChE J*. 2003;49: 969–976.
26. Li RF, Wang XZ. Dimension reduction of process dynamic trends using independent component analysis. *Comput Chem Eng*. 2002;26: 467–473.
27. Nomikos P, MacGregor JF. Monitoring batch processes using multiway principal component analysis. *AIChE J*. 1994;40:1361–1375.
28. MacGregor JF, Kourti T. Statistical process-control of multivariate processes. *Control Eng Pract*. 1995;3:403–414.
29. Russell E, Chiang LH, Braatz RD. *Data-Driven Methods for Fault Detection and Diagnosis in Chemical Processes*. London: Springer, 2000.
30. Qin SJ. Statistical process monitoring: basics and beyond. *J Chemom*. 2003;17:480–502.
31. Wold S, Esbensen K, Geladi P. Principal component analysis. *Chemom Intell Lab Syst*. 1987;2:37–52.
32. Miller P, Swanson RE, Heckler CE. Contribution plots: a missing link in multivariate quality control. *Appl Math Comput Sci*. 1998;8: 775–792.
33. Westerhuis JA, Gurden SP, Smilde AK. Generalized contribution plots in multivariate statistical process monitoring. *Chemom Intell Lab Syst*. 2000;51:95–114.
34. Dong F, Jiang ZX, Qiao XT, Xu LA. Application of electrical resistance tomography to two-phase pipe flow parameters measurement. *Flow Meas Instrum*. 2003;14:183–192.

Manuscript received Dec. 3, 2009, revision received Jun. 15, 2010, and final revision received Aug. 26, 2010.